EARTH SCIENCES
RESEARCH JOURNAL

Earth Sci. Res. J. Vol. 24, No. 2 (June, 2020): 141-151

UNIVERSIDAD NACIONAL DE COLOMBIA

SOIL MECHANICS

Variation in Rayleigh wave ellipticity as a possible indicator of earthflow mobility: a case study of Sobradinho landslide compared with pile load testing

Yawar Hussain[1] ,Martin Cardenas-Soto[2], César Moreira[3], Juan Rodriguez-Rebolledo[4], Omar Hamza[5], Renato Prado[6], Hernan Martinez-Carvajal[7], Jie Dou[8]

[1]Clemson University, South Carolina, USA

[2]Universidad Nacional Autónoma de México, Mexico.

[3]Universidade Estadual Paulista, Sao Paulo, Brazil.

[4]Universidade de Brasília, Brazil.

[5]University of Derby, United Kingdom.

[6]University of Sao Paulo, Brazil.

[7]Universidad Nacional de Colombia, Bogotá, Colombia

[8]Nagaoka University of Technology, Japan.

* Corresponding author: yawar.pgn@gmail.com

ABSTRACT

Rainfall-induced landslides pose a significant risk to communities and infrastructures. To improve the prediction of such events, it is imperative to adequately investigate the rainfall-dependent dynamics (leading to fluidization) and any associated internal sliding along shear planes within clayey slopes. Therefore, the present study adopted ambient noise analysis based on the Horizontal to Vertical Spectral Ratio (HVSR) method, to measure the seasonal variation of Rayleigh wave ellipticity as an indicator for the internal deformation and transition in the material state. The methodology was applied to an existing landslide, where variations in soil stiffness and internal sliding were expected to occur in response to rainfall. To improve the interpretation of the HVSR results (and hence the prediction of landslide' reactivation by rainfall), HVSR measurements were also conducted on a field-scale pile load test. The pile test allowed a comparison of the seismic data generated by the soil movement along shear planes. The HVSR curves of this field test showed two frequency peaks with no changes in the resonance. In comparison with the data obtained from the landslide, the resultant HVSR curves showed three frequency patterns: ubiquitous (2Hz), landslide (4-8Hz), and flat (no peak). However, the HVSR curves did not show any response to the expected seasonally induced variations in the landslide mass because of the relatively short data acquisition. Nevertheless, time-lapse HVSR is a promising technique that can complement other geophysical methods for improving landslide monitoring.

Keywords: ambient noise; HVSR; reactivation; stiffness; soil mechanics .

Variación estacional en la elipticidad de la onda Rayleigh como posible indicador de la activación de flujos de tierra, caso de estudio: deslizamiento de tierra en Sobradinho comparado con prueba de carga en pilote

RESUMEN

Los deslizamientos de tierra inducidos por lluvia representan un riesgo significativo para las comunidades y la infraestructura. Para mejorar la predicción de tales eventos, es imperativo investigar adecuadamente la dinámica generada por la lluvia que conduce a la fluidización, así como, cualquier deslizamiento interno que esté asociado y que se desarrolle a lo largo de los planos de falla dentro de los taludes arcillosos. Por lo tanto, para medir la variación estacional de la elipticidad de la onda Rayleigh, como un indicador de la deformación interna y de la transición del estado del material, el presente estudio adoptó la Relación Espectral Horizontal a Vertical (REHV) basada en el ruido ambiental. La técnica fue aplicada en un área de deslizamiento existente, donde se esperaba que ocurrieran variaciones en la rigidez del suelo y deslizamientos internos debidos a la lluvia. Para mejorar la interpretación de los resultados de la REHV y, por tanto, la predicción del deslizamiento generado por lluvia, la REHV fue calibrada en campo en una prueba de carga en pilote. La prueba en el permitió una comparación de los datos sísmicos generados por el movimiento del suelo a lo largo de los planos de falla. Las curvas REHV de esta prueba de campo mostraron dos picos de frecuencia sin cambios en la de la resonancia. En comparación con los datos obtenidos del deslizamiento de tierra, las curvas REHV resultantes mostraron tres patrones de frecuencia: ubicuo (2Hz), deslizamiento de tierra (4-8Hz) y plano (sin pico). Debido a que la recopilación de datos fue relativamente corta, las curvas REHV no mostraron ninguna respuesta a las variaciones estacionales inducidas por el deslizamiento de tierra. Sin embargo, la obtención de curvas REHV en un periodo de tiempo es una técnica prometedora que puede complementar otros métodos geofísicos para mejorar el monitoreo de deslizamientos de tierra.

Palabras clave: ruido ambiental; REHV; reactivación; rigidez; mecánica de suelos.

Record
Manuscript received: 31/08/2019
Accepted for publication: 27/03/2020

How to cite item
Hussain Y., Cardenas-Soto, M. Moreira, C., Rodriguez-Rebolledo, J., Hamza, O., Prado, R., Martinez-Carvajal, H., Dou, J. (2020). Variation in rayleigh wave ellipticity as a possible indicator of earthflow mobility: a case study of Sobradinho landslide compared with pile load testing. *Earth Sciences Research Journal*, 24(2), 141-151. DOI: https://doi.org/10.15446/esrj.v24n2.81974

ISSN 1794-6190 e-ISSN 2339-3459

https://doi.org/10.15446/esrj.v24n2.81974

Introduction

Landslides pose a threat to the global terrestrial hazards affecting many countries, for example: the Sidoarjo mudflow in Indonesia in 2006 (Wibisana, 2013), the Beichuan landslide in Chania in 2008 (Tang et al., 2011), and the Montecito mudflows in California in 2018 (Donnellan et al., 2018). Other examples include the 2008 Mw 7.9 Wenchuan earthquake causing about 200,000 coseismic landslides in China (Yunus et al., 2020), the 2004 Mw 6.8 Chuetsu and the 2018 Mw 6.6 Hokkaido earthquake-induced over 10000 landslides in Japan (Dou et al., 2020), respectively. Also, dense rainfall in mountainous terrain can seriously trigger numerous landslides in hill slopes in different countries and regions, such as China, Taiwan, Japan, Vietnam, etc. (Chang et al., 2019; Li et al., 2020; Pham et al., 2019, Fan et al., 2018). Due to the substantial human and economic losses accounted for the disastrous landslides, scientists worldwide focus on the fact of monitoring locations of future landslide events for mitigating such disasters.

In the case of Brazil, a significant number of shallow rainfall-triggered landslides have occurred (Hussain et al., 2017; Rosi et al., 2019). From 1988 to 2015, there were 733 landslides events in 243 Brazilian municipalities, with 4,000 fatalities. Economic losses and homelessness are the other social impacts of these hazardous events in the states of Rio de Janeiro, São Paulo, Minas Gerais, and Santa Catarina. The tragedies of 1966, 1967, 1985, 1988, 1995, 2008, 2009, 2010, 2011 and 2014 are historical reminders of the atrocities caused by landslides in Rio de Janeiro (Martins et al., 2018, Hussain et al., 2019a). The Sobradinho landslide (considered in this study) is an example of such events, which has superficially developed in lacustrine sediments, and whose movements were mostly controlled by water infiltration and fluvial dynamics (Hussain et al., 2017; Rosi et al., 2019).

Landslides involving sudden mobility of earthflows have been associated with two mutually inclusive mechanisms: (i) excess pore-water pressures generated along shear plane (Baum et al., 2003; van Asch and Malet, 2009; Hussain et al., 2019b) and (ii) loss of shear strength because of the increased degree of saturation (Pastor et al., 2010; Jongmans et al., 2015; Hamza and Bellis, 2008; Zhou et al., 2013, 2016). Accordingly, the mechanical behavior of the earthflows is considered a grouping of Coulomb plastic solids where the mobility is associated with distributed internal shearing that causes flow-like appearance instead of mass liquefaction (Hungr et al., 2001).

The pore water pressure assumption explains the mobility of landslide in terms of the reduction of shear strength along a slip surface (shear plane). However, in the case of clayey material, the undrained shear strength (cohesion) is not expected to reach zero. In such cases, the mobility can be better explained as a transition of a material state from solid to plastic and from plastic to fluid (i.e. solid-plastic-fluid) combined with internal sliding along shear planes. This process is called *fluidization,* which differs from liquefaction (Lowe, 1976; Bertello et al., 2018). However, the identification of such material transition and internal sliding is a challenging task, which requires continuous monitoring in order to improve landslides' prediction. For the monitoring, a continuous source of energy at high spatiotemporal resolution is required which can be provided by ambient noise (vibrations in the absence of any single source such as an earthquake).

The time-lapse spectral analysis and ambient noise interferometry (ANI), which measure Rayleigh wave ellipticity and Rayleigh wave velocity, respectively, are the two commonly adopted ambient noise-based techniques for the dynamic monitoring of landslides. In theory, both techniques allow time-lapse monitoring to identify temporal changes of these parameters (ellipticity and wave velocity) (Mainsant et al., 2012; Köhler and Weidle, 2019). However, very few attempts have been conducted in the literature, where seismic waves (Rayleigh wave) are utilized for the demarcation of such transition. In these studies (Mainsant et al., 2012; Bertello et al., 2018), a substantial drop of Rayleigh wave velocity has been observed in response to the earthflow acceleration, which is followed by a slow return to pre-disturbance of Rayleigh velocities as the landslide decelerates. However, these studies applied expensive, time-consuming and labor extensive techniques for the estimation of Rayleigh wave velocities such as time-lapse interferometry (Mainsant et al., 2012; Hussain et al., 2019c) and time-lapse active Multi-Channel Analysis of Surface Waves (MASW) (Bertello et al., 2018).

Rayleigh wave ellipticity calculated from an HVSR curve (Horizontal to Vertical Spectral Ratio) provides an alternative choice. Recently, few studies have interpreted seasonal changes in HVSR ellipticity curves as a result of the thaw-freeze cycles of an active permafrost layer (Abbott et al., 2016; Kula et al., 2018; Köhler and Weidle, 2019) and shallow rainfall-triggered landslide (Hussain et al., 2019c). The results of these studies have suggested that surface wave ellipticity (HVSR peak) might constitute a good indicator for the internal deformation and transition in material state (fluidization process) and can be used as a precursor for predicting earthflow. Therefore, the HVSR method could bear the potential to become a low-cost, passive, and non-invasive method for long-term monitoring and site characterization of landslides with high temporal resolution.

The aim of the present study is to improve the prediction of rainfall-induced landslides by understanding the rainfall-dependent dynamics (leading to fluidization) and any associated internal sliding along shear planes within clayey slopes. The study applied the HVSR monitoring on Sobradinho landslide, where variations in soil stiffness and internal sliding (fluidization process) would be expected to occur in response to rainfall events. To improve the interpretation of the HVSR results (and hence the prediction of landslide reactivation by rainfall), HVSR was also conducted to monitor a field-scale pile load test. This prototype experiment allows a similar mechanism (i.e., the development of shear planes leading to soil failure) to be observed under an increasing compression load. The pile load test would allow a comparison of the seismic data generated by the soil movement along shear planes. Moreover, the study included site characterization (landslide geometry and its stratigraphy) as well as directional analysis in order to identify any possible directional effects. This study provides a good basis for future investigation on landslides' early warning system.

Study area

The geology of the Federal District can be summarized in four lithological boundaries, according to regional stratigraphy, delineated as (base to top): (i) Paranoá (metasedimentary rocks – Meso-Neoproterozoic), Canastra (phyllites - Meso-Neoproterozoic); (ii) Araxá (schists - Neoproterozoic); (iii) Bambuí (clayed metasiltites rolled, clay and metasiltites banks - Meso-Neoproterozoic); (iv) Groups of soil or shallow colluvial deposits (pedimentary type - Quaternary) (Freitas-Silva and Campos, 1998). According to the Brazilian soil classification system, the region of the study area, Brasilia (Federal District), is comprised of a mantle of Tertiary-Quaternary age detritus-lateritic soil. The soil is composed mainly of red-yellow latosols and has high porosity and a cementitious bond type. Therefore, it has a highly unstable structure when subjected to an increased moisture or changes in the state of stresses. This soil almost always presents a volumetric change as high as the variation of these factors (referred to as a collapsible structure) (Hussain et al., 2019b).

On the slope of the study area, the channel depositions in the basin are distinguished as (i) landslide debrites due to recent rotational failure mechanism; (ii) fluvial deposits on recent riverbanks as alluvial fan deposits, colluvial, and alluvial. The detailed geology and geomorphology of the area can be found elsewhere (Hussain et al., 2019c and references therein).

Sobradinho landslide

The area of landslide is part of the Maranhão River Basin. The hydrographic network in this region is composed of a high-grade segment of the Contagem stream, which is a direct tributary of the Rio Maranhão. The main drainage system is controlled by the structural lineaments (faults and fractures) and low sinuosity, while the secondary network is typically dendritic with high sinuosity. The main watercourse is the *Ribeirão da Contagem*, but there are also small intermittent or perennial tributaries with flow rates of less than 0.005 m^3/second in the dry months of the year. The selected landslide is E-W trending roto-translational slide (Hungr et al. 2014), approximately 150 m long and about 70 m wide, located in a small vicinity called '*Rua do Mato*' (Figure 1). At the top of the landslide mass (along the main scarp), there is a small scarp in the middle created by the erosion caused by the release effects of the Contagem River (according to in-situ inspections), which is quite high during the rainy season (Hussain et al., 2019b). The Sobradinho landslide has been extensively studied with geophysical, geotechnical, and geomorphological methods. Figure 1 shows the location of the study area, the distribution of the HVSR stations and some aspects of the landslide.

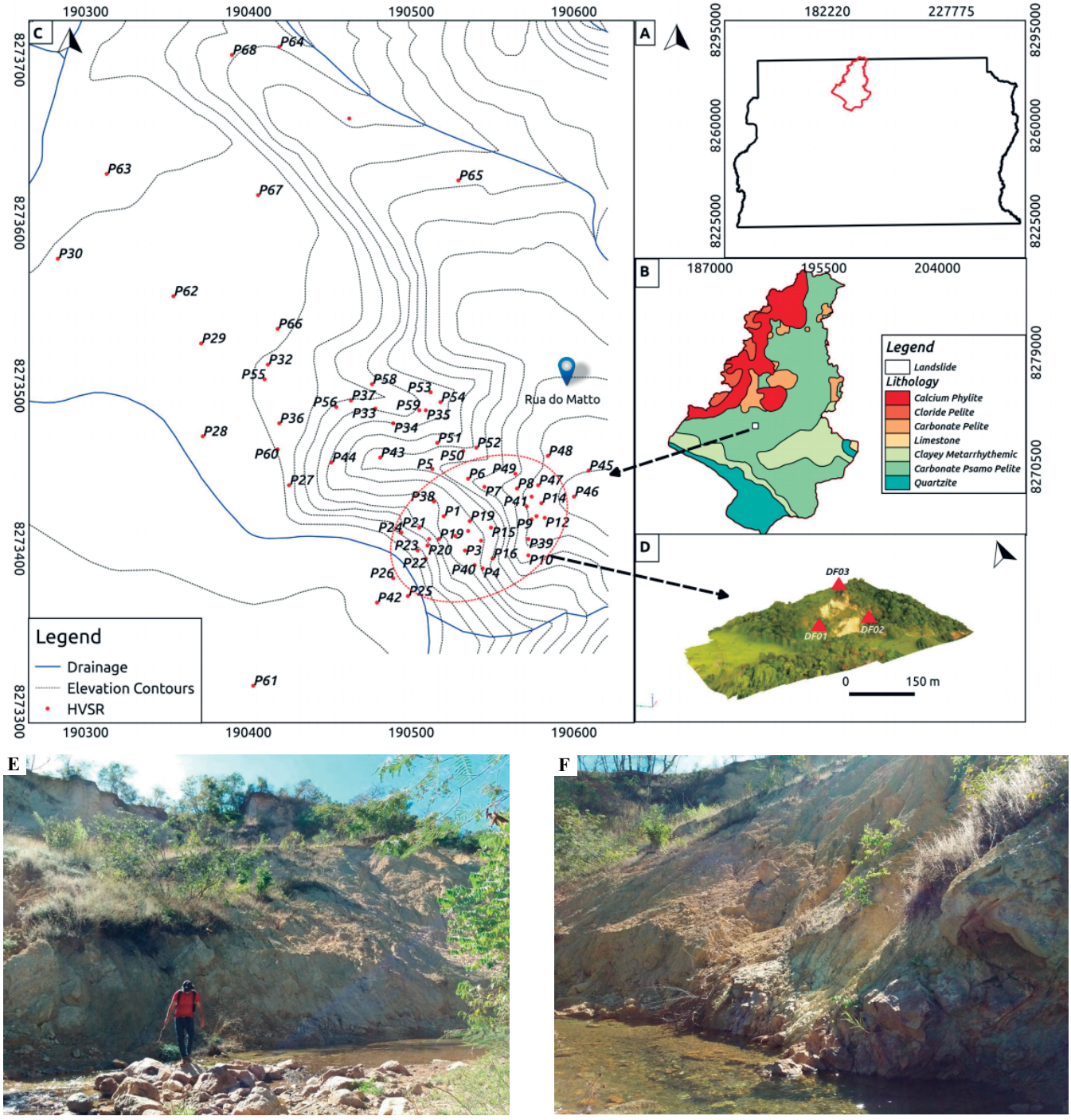

Figure 1. Location of Ribeirão Contagem watershed on Federal District map and its geology (A, B); Sobradinho landslide along the HVSR measuring points (red dots), red dashed ellipse is the approximate landslide boundary (C); Zoomed image of the landslide with a triangular array used for time-lapse monitoring (D); Photographs of the landslide (E, F).

Field scale (prototype) experiment – pile load test

Material and Methods

Pile load test (prototype experiment) was conducted in this study to artificially generate a failure mechanism with sliding of soil along shear planes at field-scale. Figure 2-A and 2-B show the location of the testing site and its soil profile. By conducting this test, our aim was to aid the interpretation of the results obtained from Sobradinho landslide. This hypothesis was based on the potential similarity of some aspects of the failure mechanisms in both cases (i.e. the landslide and the pile load test) as discussed below.

The mechanical behavior of early-stage earthflows in clayey formation might be considered as Coulomb plastic solids whose mobility is developed by sliding (as described above). In this manner, the material flows by internal deformation (internal shears) (Berti et al., 2019). So, the sliding can be resolved into several occurrences of propagation of sliding plane or soil failure (Vouillamoz et al., 2018; Hussain et al., 2019b). A similar mechanism (i.e., where shear planes are developed leading to soil failure) can be observed when a concrete pile is subjected to an increased compression force leading to soil bearing failure. However, this mechanism differs in the type and level of applied stresses, which are very small in the landslide under the influence of triggering factors (e.g. rainfall).

The fieldwork of the pile load test was conducted in several stages. In the first stage of this prototype experiment, ground characterization of the testing site was carried out using Standard Penetration Test (SPT-N). In the second stage, a concrete pile of 0.8 m diameter and 12 m depth was cast-in-situ and allowed to harden for 4 weeks. The pile was then subjected to progressive axial load while measuring the vertical displacement of the pile head. According to Brazilian standards (Hussain et al., 2019b), soil failure occurs at a displacement greater than 8 mm, where the base resistance is likely to be mobilized i.e. when shaft resistance has been or is close to being fully mobilized.

As the pile load was gradually increased at 30-minute intervals, the HVSR data was obtained from each 30-minute long ambient noise record. The pile loading mechanism was supported by two 8m deep reaction piles that balanced the applied load on the main pile. A load cell was placed below the steel rods, and a hydraulic jack was attached to the load cell. This formed a good base for applying a compression force on the pile by a manually operated oil pump. The hydraulic jack was attached to two smaller metallic rods on which four extensometers were installed for monitoring the pile vertical displacement (Figure 2C and D).

Ambient noise data acquisition at landslide area

The experimental data was acquired using Sercel L-4A-3D short period seismometers having a natural frequency response of 2 Hz. The three-component seismometer records three-dimensional ground motion in the north-south (NS), east-west (EW), and vertical (Z) directions as required by the single station HVSR analysis. For continuous data acquisition, DAS-130 REFTEK dataloggers were used that can record up to 1000 samples per second (SPS). The time and position of each measurement point were provided by the GPS-130 locks. The seismometer was aligned with the geographic north determined by a magnetic compass. The sensors were also leveled and, in order to avoid environmental interference, buried in the 50cm deep hole. The ambient noise measurements were automatically stored on two memory cards installed in the datalogger.

In the landslide experiment, the data acquisitions were conducted in two stages. In the first stage, single station HVSR measurements were taken both at the landslide mass and in the surrounding areas (Figure 1C) in order to delineate the landslide's boundary. Ambient noise at each point was recorded for 30-minutes length in accordance with the guidelines provided by SESAME (2004). In the second stage, for continuous ambient noise recording, three sensors were installed on the landslide in a triangular geometry, as adopted by Hussain et al. (2019c). The continuous data used for the seasonal impact evaluation was divided into three acquisition campaigns: (i) dry period, from 02-11-2016 to 08-11-2016; (ii) intermediate, from 12-04-2017 to 15-04-2017; and (iii) saturated period e.g. from 10-12-2017 to 17-12-2017.

HVSR technique

In the single-station HVSR technique, ambient noise recording is conducted at a single three-component station (N-S, E-W and Up-Down). The HVSR curve is interpreted in terms of its peak frequency and amplitude. The HVSR curve peak frequency is traditionally interpreted as a representative of the Rayleigh wave ellipticity or shear wave amplification over horizontally stratified layers. The physical significance of the HVSR peak amplitude is still dubious and open to debate (Fäh et al., 2001). Many authors (e.g., Bonnefoy-Claudet et al., 2008) agree on a relationship between the HVSR amplitude and the impedance contrast. Few of the documented interpretations of the peak amplitude are the reflection of ambient noise wavefield typology

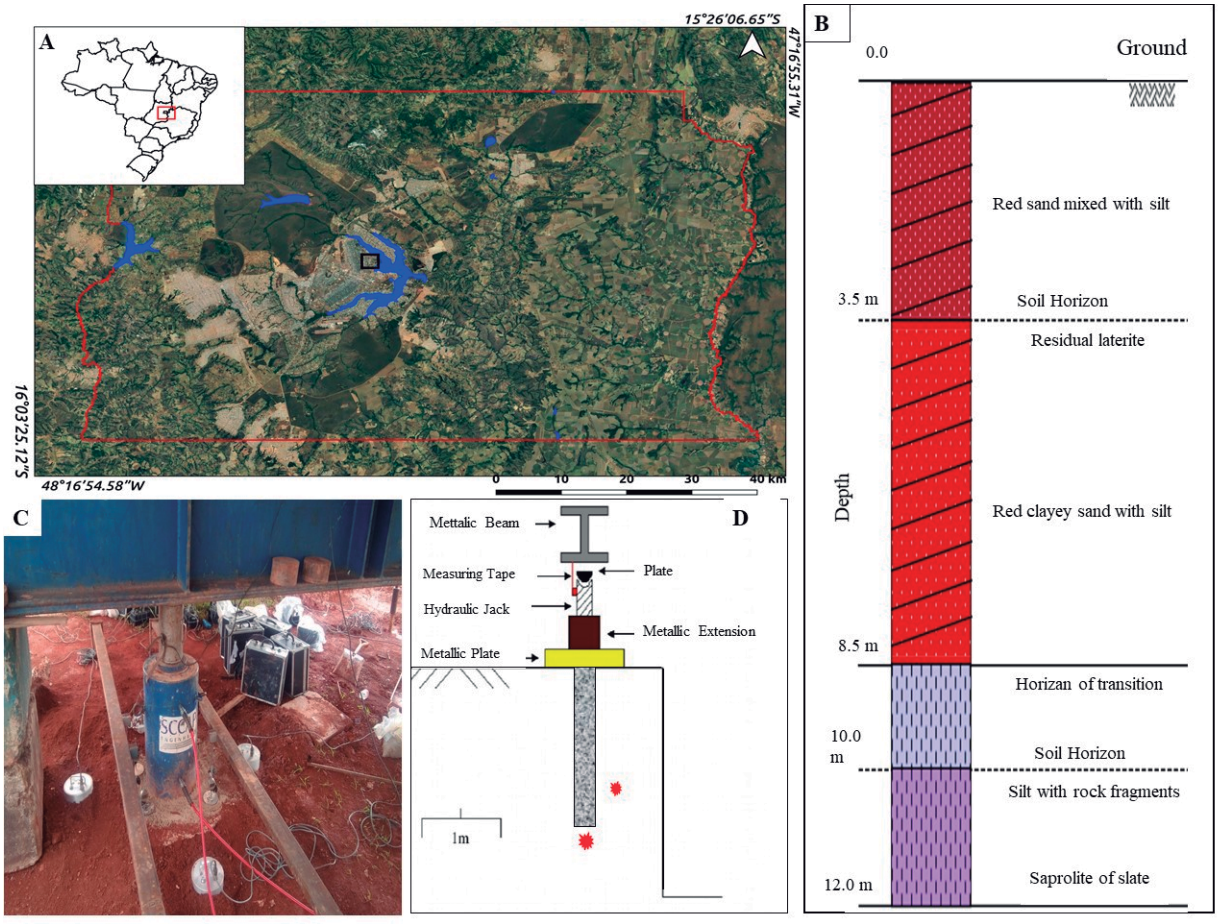

Figure 2. Prototype field experiment (pile load test) at the University of Brasilia. Location of experiment (A); Soil profile of the site (B); Photograph of the experiment (C) and Schematic of the loading mechanism (D).

(Rayleigh, Love, and body waves). However, the environmental conditions such as sensor ground coupling, water saturation (Gosar et al., 2010; Gosar and Lenart, 2010; Pazzi et al., 2018a; 2018b), weather nearby structures, underground structures, and transient noise can possibly affect the results obtained from HVSR (Chatelain et al., 2008). In a porous material, an increase of water content can influence (increase) the P-wave velocity more than Vs, thus causing an increase of Poisson ratio, which, in turn, induces an increase of Rayleigh wave ellipticity (i.e., of the H/V ratio of the elliptical particle motion). This makes the practical application of HVSR for the dynamic (fluidization) monitoring of landslide possible.

In this study, the HVSR survey was carried out in accordance with the approach provided by SESAME (2004). In this approach, the duration of ambient noise acquisition is dependent on the ambient noise levels in the area; usually, the record length should be higher than 15 minutes.

The HVSR measurements yield important insights into the resonance behavior of particular lithomorphologies and geomorphological features, while the polarization analysis of the ambient noise records can provide information about the particle motion and directivity properties, which are associated with the mechanical vibrational behavior of structures (Burjánek et al., 2012; Zare et al., 2017). The HVSR has been applied in several application including the determination of the resonance of soil deposit over the basement by Nogoshi and Igarashi (1971), earthquake hazards assessments through *microzonation* (Di Giulio et al., 2014), bedrock depth estimation (García-Jerez et al., 2006; Gosar and Lenart, 2010), archeology studies (Kalil et al., 2016), estimation of the ice sheet thickness and of the basal properties of a glacier (Picotti et al., 2017) as well as for the dynamic monitoring of glacier (Köhler et al., 2015) and landslide assessment (Imposa et al., 2017; Bertello et al., 2018, Hussain et al., 2019c). Despite these enormous applications in the last decade or so, the theoretical basis of the technique is still unclear and open to debates.

Data processing adopted in this study

The same data processing workflow was applied to the records of all experiments. The data was acquired in REFTEK format, which is first converted to a Seismic Analysis Codes (SAC) format. Then using SAC software, the data was detrended and demeaned. In the next stage, the three-component records of each point were uploaded to a freely available software Geopsy® (www.geopsy.org), where the HVSR analysis was conducted. The recorded transient events, due to any earthquakes and intermittent anthropogenic noises, were removed by choosing automatic window selection in the software. The entire length of the data was divided into short windows while performing the calculation. In the last step, the spectra were smoothened by Konno-Ohmachi function with a constant value of 40 and a cosine taper of 10% width. The entire HVSR calculation processing workflow is presented in Figure 3.

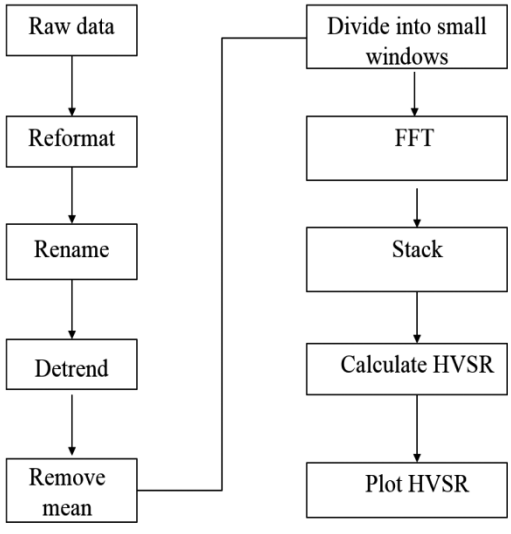

Figure 3. HVSR workflow chart of ambient noise processing in SAC and Geopsy software.

Directional analysis

While it is generally accepted that the peak frequency is reliably diagnostic of site subsoil conditions, several researchers have observed that amplitude can be considerably influenced by factors independent of site conditions e.g. the noise wavefield composition including different portions of the body, Love and Rayleigh waves (Bonnefoy-Claudet et al., 2006). The objective of the directional analysis is to understand how the landslide body receives a contribution of ambient noise energy along the different axis. If the amplification at two horizontal components is unequal with larger motion at a specific azimuthal, this is known as directional amplification (Bonamassa and Vidale, 1991). The presence of fractures and cracks as well as fault zones may show directionality. The directional amplification is suggested to be due to the presence of large-scale open cracks (Moore et al., 2011) or microcracks (Pischiutta et al., 2017). In this way, links between the distribution of noise sources and the subsurface conditions are evaluated. The analysis of directional effects in the site response is conducted by rotating the components of the spectral ratios obtained at each measurement site by steps of 10◦, starting from 0◦N to 180◦N, and plotting the contours of spectral amplitude as a function of frequency and direction of motion (Panzera et al., 2012). The 0° stands for the North direction marked on seismometer and 180° stands for South (from 0° to 360° results are symmetric). The directional effects of landslide-affected areas have been shown in previous studies (Burjánek et al., 2010; Imposa et al., 2017).

Results and Discussions

Pile load test

The results of the pile load test showed three peaks on HVSR curves: first at 5 Hz (deep interface), second at 32 Hz (not considered), and third at 55Hz (shallow interface). Both peaks (shallow and deep) represent the depth of soil horizons, i.e., shallow and deep interfaces. Following an 1D simple modeling, a site resonance frequency *fo* was related to the thickness *h* of surface material having velocity Vs through the following equation:

$$fo=Vs/4h \quad (1)$$

The Vs value is calculated from SPT-N using Imai et al. (1977) relation for all soils as 550 m/s, which for fo=5 Hz would imply a thickness of less than 30 m. Assuming a value of 55Hz for the relevant peak, the thickness of the material involved in resonance would be 2.5 m, i.e. a thin surface soil layer (Hussain et al., 2019d). Both peaks show variations in their amplitudes with the increase of an applied load with constant resonance frequency. According to the results shown in Figure 4 (A), the variations of the mean amplitude measured on successive time intervals of 30 minutes were very small and did not follow a trend correlated to the load increase. These variations are most likely irrelevant to the changes in soil mechanical properties; it seems that they depend on the variations in ambient noise wavefield composition recorded over time. There was another HVSR peak at a frequency range of 32Hz, having peak amplitude rather low, not reaching an HVSR factor of 2, which is generally considered a minimum threshold to infer the occurrence of significant resonance phenomena (see SESAME-2004 guidelines); thus, this peak was not considered for the analysis.

The geometrical similarities of the curves revealed that the peak frequency of HVSR curves at all time steps were similar. This might be attributed to the presence of identical subsurface stratigraphy (the same impedance contrast), which did not change with the applied load. The shear sliding (internal sliding) in the soil was too small to mark any difference in the HVSR curve peak, although other studies have also documented such changes in peak ambient under different phenomena (e.g., Köhler et al. 2006; Bonnefoy-Claudet et al., 2008).

The recorded low-frequency resonance peak (5Hz) is almost azimuth independent (as shown in A-H in Figure 5), denoting the absence of 2-D effects. The stratigraphic peak did not show any variation with azimuth, while the higher frequency peak showed azimuthal dependent variations (Figure 5). The prominent azimuth range was 20-60 and 100-180, implying the non-uniform distribution of ambient noise sources surrounding the sensor.

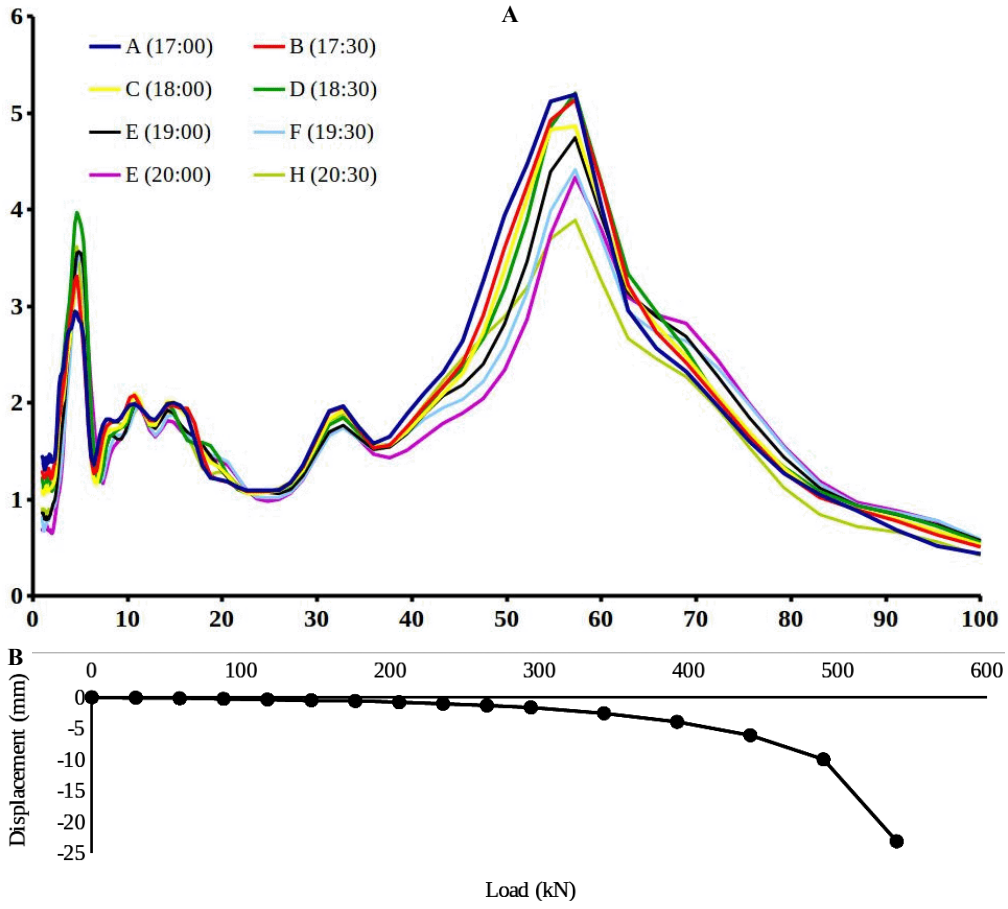

Figure 4. Results of the pile load test: (A) The HVSR curves obtained at each loading increment (30 minutes). Three peaks were observed: first (5Hz), second (32Hz), and third (55Hz), (B) The load-displacement curve of the pile compression load test.

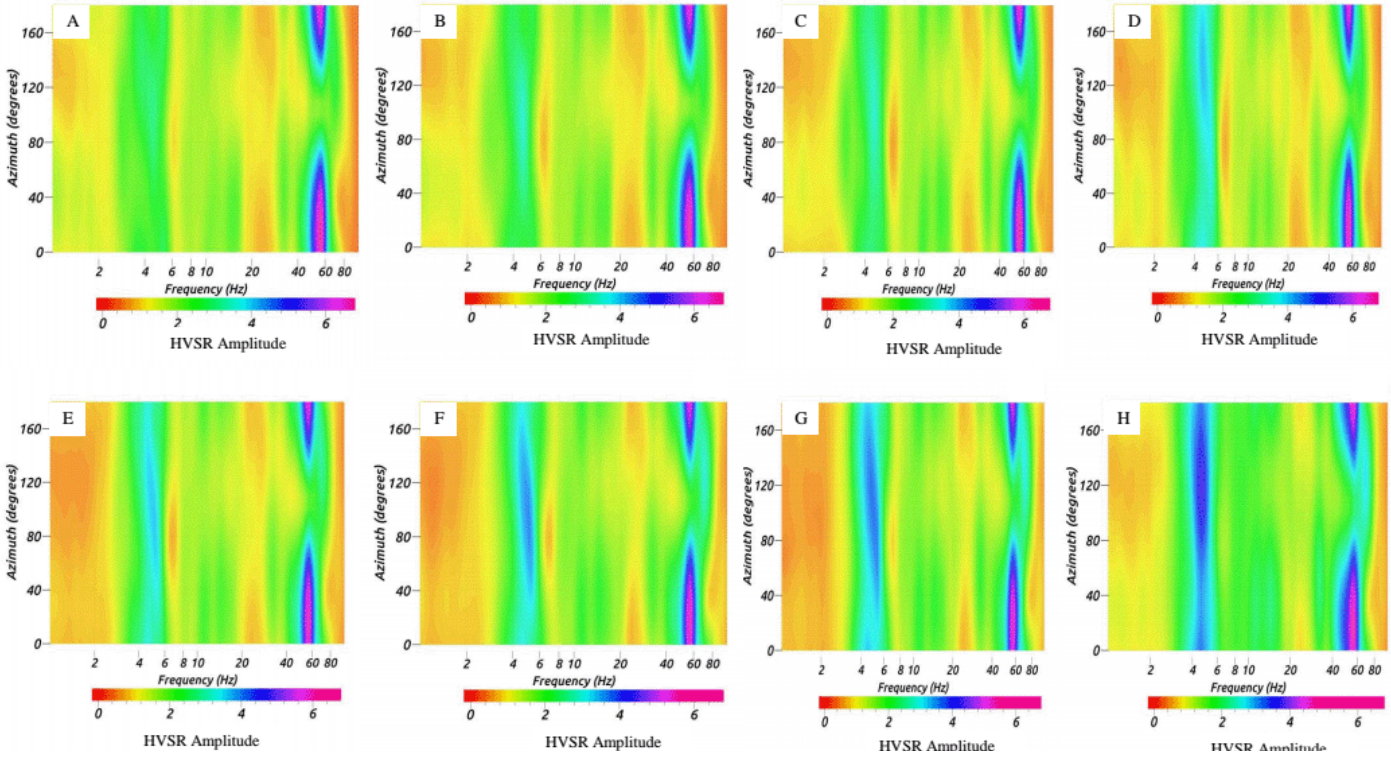

Figure 5. Directional analysis of each 30 minutes long files (A, B, C, D, E, F, G, and H). Each figure shows the contour plots of the HVSR curve as a function of frequency (x-axis) and rotation angle (y-axis) with respect to the geographic north. The color scale represents the HVSR amplitude.

Landslide monitoring

Ubiquitous frequency

The ubiquitous frequency was the frequency of saprolite (highly weathered rock), the soft layer over the seismic bedrock, and it was generally recorded throughout the studied area having high amplitude relative to the landslide peak (Figures 5A, 6 and 7). This peak was not affected by the seasonal variations (stiffness) produced by meteorological changes (degree of saturation). However, there were slight variations in peak amplitude recorded at different points in the study area (Figures 6 and 7) that could be linked with the composition of ambient noise wavefield. Based on the active MASW results of a study carried out by Hussain et al. (submitted), the value of shear wave velocity was considered as 160 m/s. This value is low because of the high porosity of material and disturbance brought by the onset of the landslide. Using the equation (1) with Vs=160 m/s and h = the thickness of the sediment package over the seismic bedrock, it was found that the thickness of the saprolite plus clay layer is 20m deep. These results are consistent with the results obtained by joint inversion of HVSR and f-k curves, where the depth of Saprolite was found equal to 23 m (Hussain et al., 2019d).

The ubiquitous frequency did not show the amplitude variations of the HVSR along the azimuths, mainly because it represented the stratigraphy and not the fractured landslide mass that led to trap seismic energy at a particular direction (azimuth) (Zare et al., 2017; Rezaei et al., 2018). We observed that the rotated HVSR obtained in the landslide fractured zones showed clear directional effects, which were quite complex and could not be interpreted easily. There were two groups on the HVSR curves: 1) where the amplitude is similar in almost all directions (2Hz peak), and 2) where the higher amplitudes of the landslide peak (higher peak) are between 40° and 150° (Figure 6). It is possible that can provide some more conformation about the ambient source distributions or the presence of fractures linked with the landslide boundary.

Landslide frequency

In Figures 6 and 7 along the high amplitude stratigraphic peak (2 Hz), there are peaks at higher frequencies having low amplitudes, which presumably indicate the presence of shallower velocity boundaries within the sediments. The amplitudes of these side peaks were, in most cases, considerably lower than the amplitude of the main peak; only at P5 and P11, the amplitudes were higher. This relatively low amplitude over the HVSR curve secondary peak is mainly related to the presence of thin and soft soil covers (Stanko et al., 2017). The presence of such peaks has also been reported in previous studies (Gosar and Lenort, 2010). The variation in amplitude is possibly related to the ambient noise sources in the region and the contribution of Love waves that affect the amplitude of the H/V peak, as described in section 4.1. These higher frequency peaks 6Hz and 8Hz represent landslide depth (slip surface) at 6.6 m and 5 m, respectively. The depth of the slip surface is relatively consistent with the usual depth surface of the landslides in the region.

The higher resonance frequencies represent the detached soil blocks created by the seasonal erosion of the Contagem River flowing at the bottom. The river crosses the landslide at the bottom, which is a possible source of disturbance (dynamism) in the landslide mass. As a result, fractures are produced; some of these fractures are very deep, supported by visual field inspections – conducted by the authors. Each block has its own degree of freedom and has a different resonance frequency, which may explain the emergence of secondary peaks of different frequencies depending on the location along the landslide (Figure 6, 7). The emergency of stratigraphic and landslide peaks has been reported in a previous study by Rezaei et al. (2018) at a landslide in Tehran, Iran.

Flat HVSR

This class of HVSR curves lacked any frequency peak according to the reliability criteria of clear peak (amplitude greater than 2). There are two possible reasons for the absence of a peak on HVSR curves (i) bedrock are exposed or (ii) low-quality data. At some locations, the secondary peak also appeared with very low amplitude because of the presence of coarser grain material towards the floodplain of the river that lies behind the landslide. These curves were not considered for the analysis. The results are shown in Figure 8.

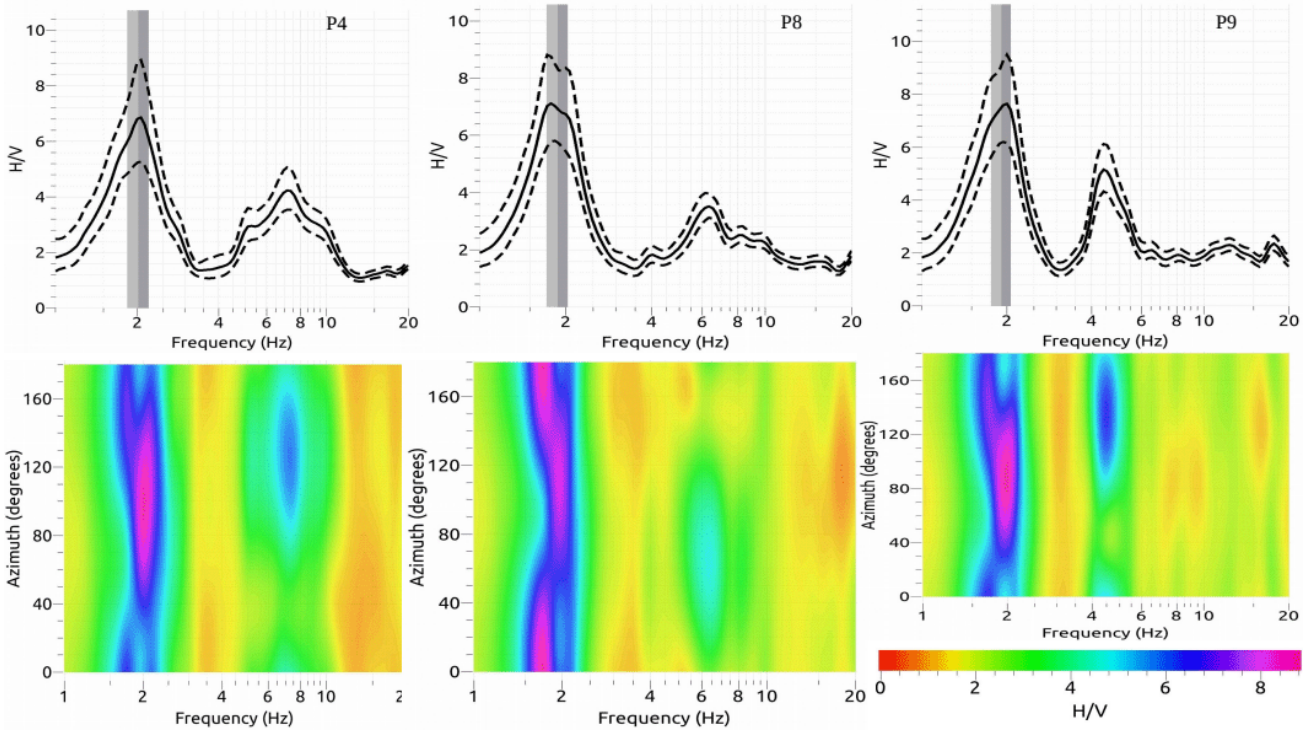

Figure 6. HVSR curves of group-A Peak at 2 Hz and 4-6 Hz. The two dashed lines represent the HVSR standard deviation, while the gray areas represent the peak frequency standard deviation, which quantifies the experimental error associated with the average peak frequency value. Below we show the contour plots of HVSR curves as a function of frequency (x-axis) and rotation angle (y-axis) with respect to the geographic north. The color scale represents the HVSR amplitude.

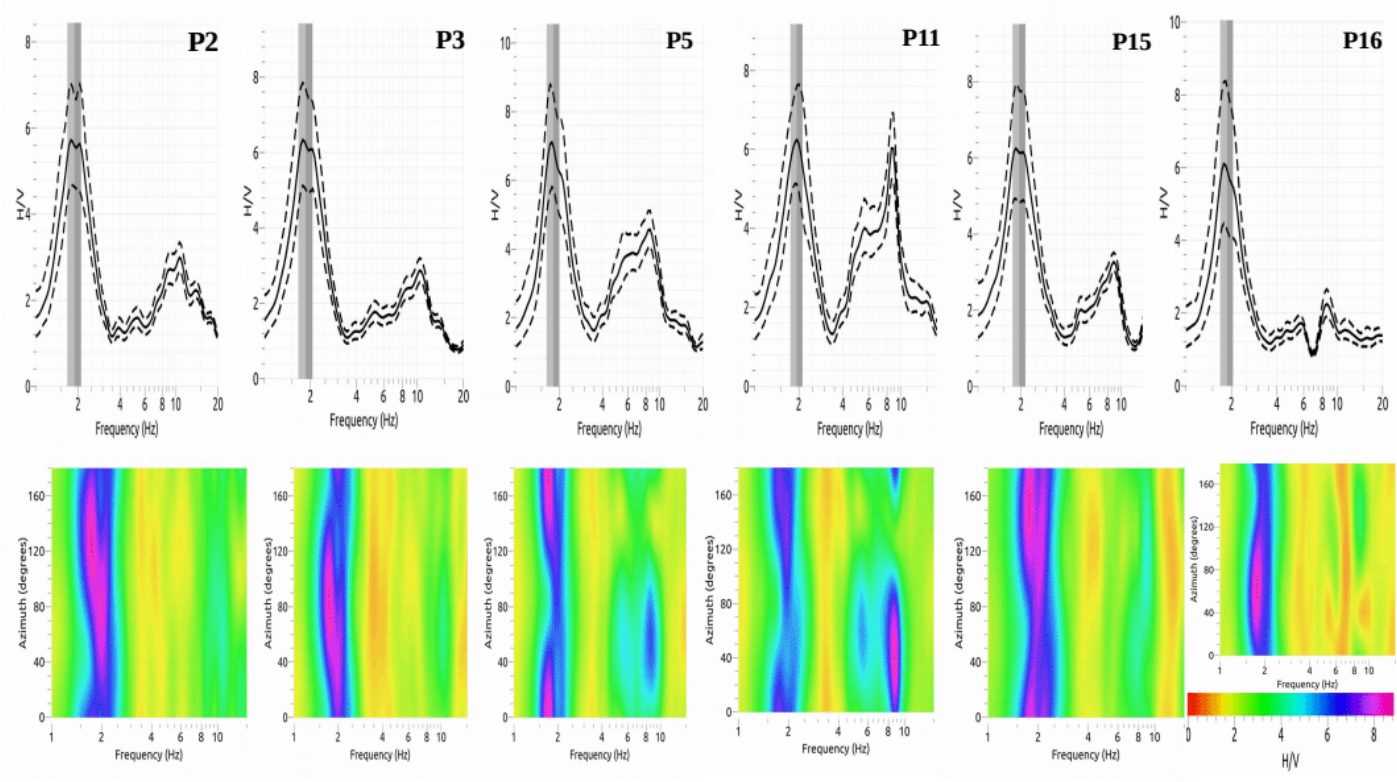

Figure 7. HVSR curves of group-B peak at 2 Hz and 8-10Hz (P refers to HVSR station, Figure 1). Legend is the same as of Figure 5. The color bar presents the HVSR amplitude.

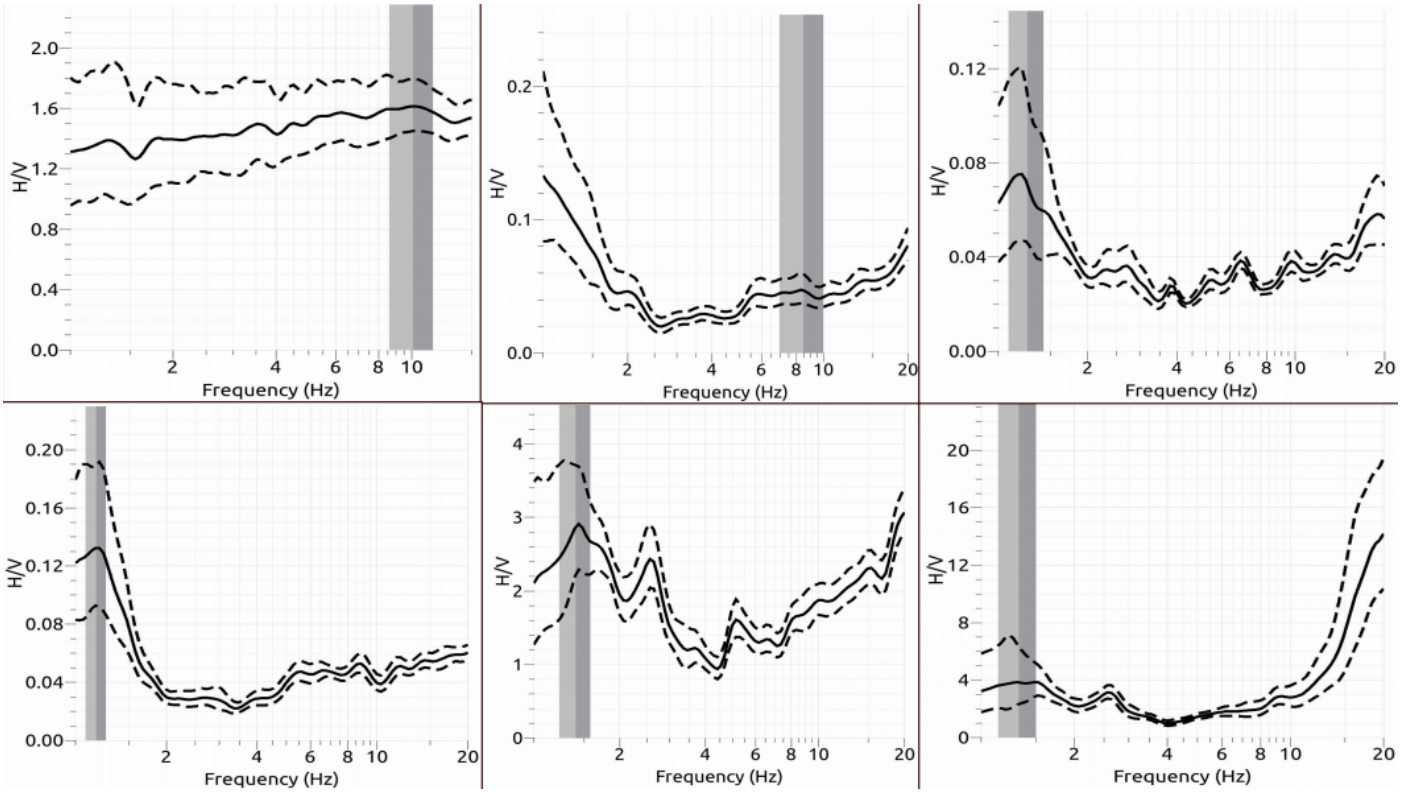

Figure 8. No peak/flat response of the strata on the HVSR curves. HVSR standard deviation, while the gray areas represent the peak frequency standard deviation, which quantifies the experimental error associated with the average peak frequency value.

Degree of saturation

The effects of rainfall infiltration are possibly related to changes in the Poisson ratio that affects Rayleigh wave ellipticity (HVSR). The changes in Rayleigh wave ellipticity may also be related to the rise in pore pressures in the landslide mass, internal sliding, and changes in the state of landslide mass (as described in section1). In addition to the reduction of the soil stiffness due to the pore water pressure, the filtered water can reduce the shear wave velocity through increasing the degree of saturation. These phenomena have extensively been studied in the landslides triggered by rainfall and earthquakes (Mainsant et al. 2012; Harba and Pilecki, 2017; Hussain et al., 2019b; 2019c).

The results of the present study did not show changes in the ubiquitous and higher frequency peaks and their amplitudes in response to rainfall dependent degree of saturation (Figure 9, 10). One possible reason as documented by Hussain et al. (2019c), is the insufficient amounts of rainfall recorded during the shorter data acquisition campaigns. These conditions did not let the highly porous landslide mass to reach high saturation levels.

At station DF01, no secondary peak was observed, and only stratigraphic peak appeared. This station was located in a stable place. The peak showed no variations in response to meteorological changes (Figure 9). The records of station DF02 showed a well-defined HVSR peak at higher frequency (landslide peak). This higher peak was present throughout the entire length of the experiment irrespective of the day-night ambient noise variabilities (Figure 10). However, there was no evidence of the changes in the resonance of landslide with rain, which showed the absence of dynamism (e.g., fluidization or internal sliding) in the landslide mass.

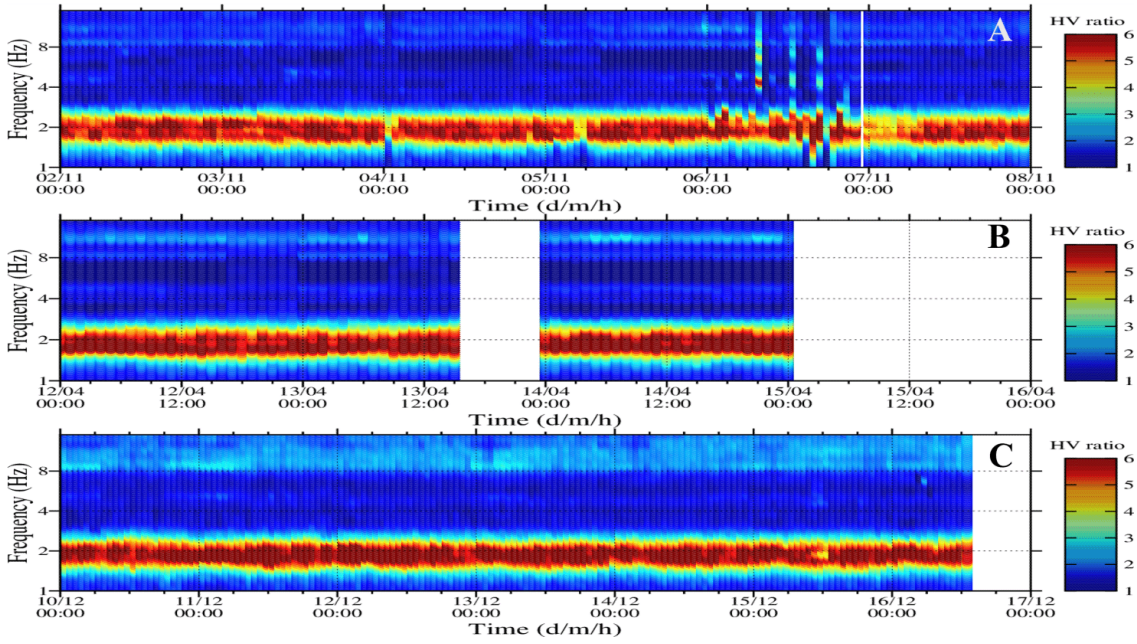

Figure 9. The response of HVSR curves because of the degree of saturation recorded at triangular array of three sensors. Color presents HVSR amplitude. Station DF01: (A) dry period, from 02-11-2016 to 08-11-2016; (B) intermediate, from 12-04-2017 to 15-04-2017; (C) saturated period e.g., from 10-12-2017 to 17-12-2017.

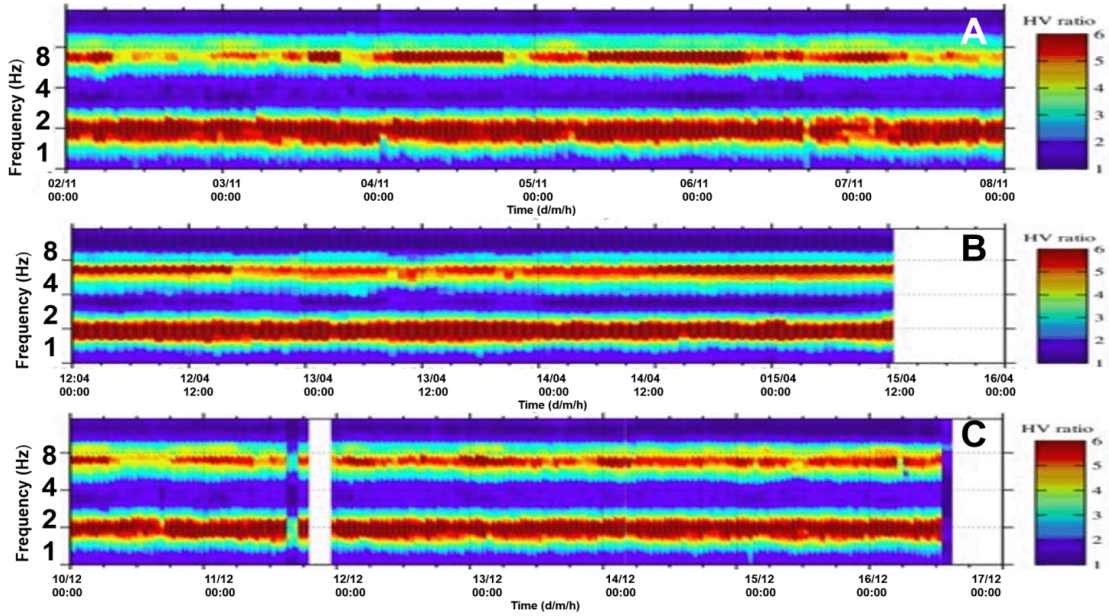

Figure 10. The response of HVSR curves to the degree of saturation recorded at the triangular array of three sensors. Color presents HVSR amplitude. Station DF02: (A) dry period, from 02-11-2016 to 08-11-2016; (B) intermediate, from 12-04-2017 to 15-04-2017; (C) saturated period e.g., from 10-12-2017 to 17-12-2017.

Conclusions

The HVSR results obtained from the landslide showed several peaks. In particular, the ubiquitous peak at low frequency (2Hz) was not related to landslide dynamics. Instead, it represented the site response of seismically low-velocity soil layer overlying higher velocity Saprolite (20m deep). Whereas the landslide peaks at high frequency were related to the detached blocks at the landslide mass and their amplitudes reflected the degree of impedance contrasts created by either the presence of thin, soft sediments or the composition of ambient noise wavefield. Both peaks (ubiquitous and landslide) did not show any response to the effects of rainfall, mainly because of the relatively small degree of soil saturation. In comparison, the pile load test showed two stratigraphic peaks, for every increase in soil stress there was a small variation in the amplitudes of the HVSR peaks, which might be related to the composition of ambient noise wavefield,

Overall, these observations suggest that HVSR amplitude variabilities were complex and created by the structural change in the shallow sub-surface and the ambient noise wavefield composition. The variability reflected local noise conditions at each individual station affected by topography, vicinity to streams (Contagem River), exposure to wind, and extend and timing of degrading instrument coupling. Therefore, our data did not allow precise identification of the relationship between rainfall-induced dynamic (fluidization), displacement rate, and Rayleigh ellipticity. However, it was still possible to conduct the landslide site characterization using limited ambient noise data.

The present study provides a sound basis for a more comprehensive application of seismic noise measurements, a potential method in the disaster diagnosis and prediction, with an emphasis in densely populated mountainous areas. Further investigation is recommended where greater deformations and larger scale fractures (centimeters) can be created in the soil in order to identify the possible effects of soil deformations on HVSR. The study can also benefit from the development of an improved physical simulation of the emergence and propagation of fractures as well as the fall of soil blocks in order to determine the possible effects of the landslide - before, during and after the event. Moreover, these results can be validated by conducting remote sensing of the landslide surface to confirm the actual movement of the soil mass.

Acknowledgment

The authors acknowledge the support of the following agencies: the National Council for Scientific and Technological Development (CNPq), the Support Research of the Federal District Foundation (FAP-DF), the University of Brasilia and, the Pool of Brazilian Equipments (PegBr), Rio de Janeiro.

References

Baum, R. L., Savage, W. Z., & Wasowski, J. (2003). Mechanics of Earth Flows. Paper presented at International Workshop on Occurrence and Mechanisms of Flows in Natural Slopes and Earthfills, Sorrento, Italy.

Bertello, L., Berti, M., Castellaro, S., & Squarzoni, G. (2018). Dynamics of an Active Earthflow Inferred From Surface Wave Monitoring. *Journal of Geophysical Research: Earth Surface*, 123(8), 1811-1834.

Berti, M., Bertello, L., & Squarzoni, G. (2019). Surface-wave velocity measurements of shear stiffness of moving earthflows. *Landslides*, 16(3), 469-484.

Bonamassa, O., & Vidale, J. E. 1991. Directional site resonances observed from aftershocks of the 18 October 1989 Loma Prieta earthquake. *Bulletin of the Seismological Society of America*, 81(5), 1945-1957.

Bonnefoy-Claudet, S., Cotton, F., & Bard, P. Y. (2006). The nature of noise wavefield and its applications for site effects studies. A literature review. *Earth-Science Reviews*, *79*(3-4), 205-227.

Bonnefoy-Claudet, S., Köhler, A., Cornou, C., Wathelet, M., & Bard, P. Y. (2008). Effects of Love waves on microtremor H/V ratio. *Bulletin of the Seismological Society of America*, 98(1), 288-300.

Braga, L. M., Caldeira, D., da Silva Nunes, J. G., Hussain, Y., Carvajal, H. M., & Uagoda, R. (2018). Caracterização geomorfológica e dinâmica erosivo-deposicional de encostas no vale fluvial do Ribeirão Contagem-DF, Brasil. *Anuário do Instituto de Geociências – UFRJ,* 41(2), 51-65.

Burjánek, J., Gassner-Stamm, G., Poggi, V., Moore, J.R., & Fäh, D. (2010). Ambient vibration analysis of an unstable mountain slope. *International Journal of Geophysics*, 180(2), 820–828.

Burjánek, J., Moore, J. R., Yugsi-Molina, F. X., & Fäh, D. (2012). Instrumental evidence of normal mode rock slope vibration. *Geophysical Journal International*, 188, 559–569.

Chang, K. T., Merghadi, A., Yunus, A. P., Pham, B. T., & Dou, J. (2019). Evaluating scale effects of topographic variables in landslide susceptibility models using GIS-based machine learning techniques. *Scientific Reports,* 9, 12296. https://doi.org/10.1038/s41598-019-48773-2

Chatelain, J. L., Guillier, B., Cara, F., Duval, A. M., Atakan, K., & Bard, P. Y. (2008). Evaluation of the influence of experimental conditions on H/V results from ambient noise recordings. *Bulletin of Earthquake Engineering*, 6(1), 33-74.

Donnellan, A., Parker, J., Milliner, C., Farr, T. G., Glasscoe, M., Lou, Y., Zheng, Y., & Hawkins, B. (2018). UAVSAR and optical analysis of the Thomas fire scar and Montecito debris flows: Case study of methods for disaster response using remote sensing products. *Earth and Space Science*, 5(7), 339-347.

Dou, J., Yunus, A. P., Merghadi, A., Shirzadi, A., Nguyen, H., Hussain, Y., Avtar, R., Chen, Y. L., Pham, B. T., & Yamagishi, H. (2020b). Different sampling strategies for predicting landslide susceptibilities are deemed less consequential with deep learning. *Science of the Total Environment,* 137320. https://doi.org/10.1016/j.scitotenv.2020.137320

Fäh, D., Kind, F., & Giardini, D. (2001). A theoretical investigation of average H/V ratios. *Geophysical Journal International*, 145(2), 535-549.

Fan, X., Zhan, W., Dong, X., van Westen, C., Xu Q., Dai, L., Yang, Q., Huang, R., & Havenith, H. B. (2018). Analyzing successive landslide dam formation by different triggering mechanisms: The case of the Tangjiawan landslide, Sichuan, China. *Engineering geology*, 4(243), 128-144.

Freitas-Silva, F. H., & Campos, J. E. G. (1998). *Geologia do Distrito Federal*. In: IEMA/SEMATEC/UnB 1998. Inventário Hidrogeológico e dos Recursos Hídricos Superficiais do Distrito Federal. Brasília. IEMA/SEMATEC/UnB. Vol. 1, Part I. P86.

García-Jerez A., Luzón F., Navarro M., Pérez-Ruiz J.A. (2006). Characterization of the sedimentary cover of the Zafarraya basin, southern Spain, by means of ambient noise. *Bulletin of the Seismological Society of America*, 96(3), 957-967.

Gosar, A., & Lenart, A. (2010). Mapping the thickness of sediments in the Ljubljana Moor basin (Slovenia) using microtremors. *Bulletin of Earthquake Engineering*, 8(3), 501-518.

Gosar, A., Rošer, J., Motnikar, B. Š., & Zupančič, P. (2010). Microtremor study of site effects and soil-structure resonance in the city of Ljubljana (central Slovenia). *Bulletin of earthquake engineering*, 8(3), 571-592.

Hamza, O., & Bellis A. (2008). *Gault Clay embankment slopes on the A14–Case studies of shallow and deep instability.* In Advances in Transportation Geotechnics: Proceedings of the International Conference held in Nottingham, UK, 25-27 August 2008 (p. 307). CRC Press.

Harba, P., & Pilecki, Z. (2017). Assessment of time–spatial changes of shear wave velocities of flysch formation prone to mass movements by seismic interferometry with the use of ambient noise. *Landslides*, 14(3), 1225-1233.

Hungr, O., Evans, S. G., Bovis, M. J., Hutchinson, J. N. (2001). A review of the classification of landslides the flow type. *Environmental and Engineering Geoscience*, 7, 221-238.

Hungr, O., Leroueil, S., & Picarelli, L. (2014). The Varnes classification of landslide types, an update. *Landslides*, 11(2), 167-194.

Hussain, Y., Cardenas-Soto, M., Uagoda, R., Martino, S., Rodriguez-Rebolledo, J., Hamza, O., & Martinez-Carvajal, H. (2019c). Monitoring of Sobradinho landslide (Brasília, Brazil) and a prototype vertical slope by time-lapse interferometry. *Brazilian Journal of Geology*, 49(2), e20180085.

Hussain, Y., Cardenas-Soto, M., Uagoda, R., Martino, S., Sanchez, N. P., Moreira, C. A., Martinez-Carvajal, H. (2019d). Shear Wave Velocity Estimation by a Joint Inversion of HVSR and f-k Curves under Diffuse Field Assumption: A Case Study of Sobradinho Landslide. *Anuário do Instituto de Geociência*, 42(1/2019), 742-775.

Hussain, Y., Hussain, S. M., Cardenas-Soto, M., Uagoda, R., Martino, S., Rodriguez-Rebolledo, J., Hamza, O., Martinez-Carvajal, H. (2019b). Typological analysis of slidequakes emitted from landslides: experiments on an expander body pile and Sobradinho landslide (Brasilia, Brazil). *REM-International Engineering Journal*, 72(3), 453-460.

Hussain, Y., Martinez-Carvajal, H., Cárdenas-Soto, M., Uagoda, R., Martino, S., Hussain, B. M. (2017). Microtremor Response of a Mass Movement in Federal District of Brazil. *Anuário do Instituto de Geociências*, 40(3), 212-221.

Hussain, Y., Martinez-Carvajal, H., Condori, C., Uagoda, R., Cárdenas-Soto, M., Cavalcante, A. L. B., Da Cunha, L. S., Martino S. (2019a). Ambient Seismic Noise: A Continuous Source for the Dynamic Monitoring of Landslides. *Terrae Didatica*, 15(01), 103-107.

Imai, T., & Tonouchi, K. (1982). *Correlation of N-value with S-wave velocity and shear modulus*. Penetration testing: proceedings of the second European symposium on penetration testing, (Amsterdam), 57–7.

Imposa, S., Grassi, S., Fazio, F., Rannisi, G., & Cino, P. (2017). Geophysical surveys to study a landslide body (north-eastern Sicily). *Natural Hazards*, 86(2), 327-343.

Jongmans, D., Baillet, L., Larose, E., Bottelin, P., Mainsant, G., Chambon, G., & Jaboyedoff, M. (2015). *Application of ambient vibration techniques for monitoring the triggering of rapid landslides.* Paper presented at Engineering Geology for Society and Territory, Torino, Italy.

Kalil, A. E., Abdel, H. E., & Mossa, H. (2016). The efficiency of horizontal to vertical spectral ratio technique for buried monuments delineation (case study, Saqqara (Zoser) pyramid, Egypt). *Arabian Journal of Geosciences*, 9(1), 1-9.

Köhler, A., Nuth, C., Schweitzer, J., Weidle, C., & Gibbons, S. J. (2015). Regional passive seismic monitoring reveals dynamic glacier activity on Spitsbergen, Svalbard. *Polar Research*, 34(1), 26178.

Li, H., Xu, Y., Zhou, J., Wang, X., Yamagishi, H., & Dou, J. (2020). Preliminary analyses of a catastrophic landslide occurred on July 23, 2019, in Guizhou Province, China. *Landslides,* 17, 719–724. https://doi.org/10.1007/s10346-019-01334-0

Lowe, D. R. (1976). Subaqueous liquefied and fluidized sediment flows and their deposits. *Sedimentology*, *23*(3), 285-308.

Mainsant, G., Jongmans, D., Chambon, G., Larose, E., & Baillet, L. (2012). Shear-wave velocity as an indicator for rheological changes in clay materials: Lessons from laboratory experiments. *Geophysical Research Letters*, 39(19).

Martins, T. D., Vieira, B. C., Fernandes, N. F., Oka-Fiori, C., & Montgomery, D. R. (2017). Application of the SHALSTAB model for the identification of areas susceptible to landslides: Brazilian case studies. *Revista de Geomorfologie*, 19, 136-144.

Moore, J. R., Gischig, V., Burjánek, J., Loew, S., & Fäh, D. (2011). Site effects in unstable rock slopes: dynamic behavior of the Randa instability (Switzerland). *Bulliten of Seismological Society America*, 101.

Nogoshi, M., & Igarash, T. (1971). On the amplitude characteristics of microtremor (Part 2). *Journal of the Seismological Society of Japan*, 24(1), 26-40.

Nunes, J. G. S., Caldeira, D., Braga, L. M., Hussain, Y., Carvajal, H. M., & Uagoda, R. (2019). Aplicação do GPR Para Análise e Diferenciação entre Materiais Aluvionares e Coluvionares, Embasadas em Observações Diretas, no Vale do Ribeirão Contagem-Distrito Federal (in Purtuguese), *Revista Brasileira de Geomorfologia*, 20(2), 217-238.

Panzera, F., D'Amico, S., Lotteri, A., Galea, P., & Lombardo, G. (2012). Seismic site response of unstable steep slope using noise measurements: the case study of Xemxija bay area, Malta. *Natural Hazards and Earth System Sciences*, 12(11), 3421.

Pastor, M., Manzanal, D., Fernandez Merodo, J. A., Mira, P., Blanc, T., Drempetic, V., Pastor M. J., Haddad, B., Sanchez, M. (2010). From solids to fluidized soils: diffuse failure mechanisms in geostructures with applications to fast catastrophic landslides. *Granular Matter*, 12(3), 211-228.

Pazzi, V., Ceccatelli, M., Gracchi, T., Masi, E. B., Fanti, R. (2018b). Assessing subsoil void hazards along a road system using H/V measurements, ERTs, and IPTs to support local decision makers. *Near Surface Geophysics*, 16, 282-297.

Pazzi, V., Di Filippo, M., Di Nezza, M., Carlà, T., Bardi, F., Marini, F., Fontanelli, K., Intrieri, E., Fanti, R. (2018a). Integrated geophysical survey in a sinkhole-prone area: microgravity, electrical resistivity tomographies, and seismic noise measurements to delimit its extension. *Engineering Geology*, 243, 282-293.

Pazzi, V., Tanteri, L., Bicocchi, G., D'Ambrosio, M., Caselli, A., & Fanti, R. (2017). H/V measurements as an effective tool for the reliable detection of landslide slip surfaces: case studies of Castagnola (La Spezia, Italy) and Roccalbegna (Grosseto, Italy). *Physics and Chemistry of the Earth, Parts A/B/C*, 98, 136-153.

Pham, B. T., Prakash, I., Dou, J., Singh, S. K., Trinh, P. T., Tran, H. T., Le, T. M., Van Phong, T., Khoi, D. K., Shirzadi, A., & Bui, D. T. (2019). A novel hybrid approach of landslide susceptibility modelling using rotation forest ensemble and different base classifiers. Geocarto Interational, 1–25. https://doi.org/10.1080/10106049.2018.1559885

Picotti, S., Francese, R., Giorgi, M., Pettenati, F., & Carcione, J. M. (2017). Estimation of glacier thicknesses and basal properties using the horizontal-to-vertical component spectral ratio (HVSR) technique from passive seismic data. *Journal of Glaciology*, 63(238), 229-248.

Pischiutta, M., Fondriest, M., Demurtas, M., Magnoni, F., Di Toro, G., & Rovelli, A. (2017). Structural control on the directional amplification of seismic noise (Campo Imperatore, central Italy). *Earth and Planetary Science Letters*, 471, 10-18.

Rezaei, S., Shooshpasha, I., Rezaei, H. (2018). Evaluation of landslides using ambient noise measurements (case study: Nargeschal landslide). *International Journal of Geotechnical Engineering, 1–11.*

Rosi, A., Canavesi, V., Segoni, S., Dias Nery, T., Catani, F., & Casagli, N. (2019). Landslides in the Mountain Region of Rio de Janeiro: A Proposal for the Semi-Automated Definition of Multiple Rainfall Thresholds. *Geosciences*, 9(5), 203.

Sesame (2004). Guidelines for the Implementation of the H/V Spectral Ratio Technique on Ambient Vibrations. Measurements, Processing and Interpretation. SESAME European Research Project WP12—D23.12. http://sesame-fp5.obs.ujf-grenoble.fr/ Papers/HV_User_Guidelines.pdf.

Silva, M. T. M. G. (2009). Metodologia para determinação de parâmetros para solos não saturados utilizando ensaios com umidade conhecida. MSc. Dissertation, Universidade de Brasília, Brasília, Brazil.

Stanko, D., Markušić S., Strelec, S., & Gazdek, M. (2017). HVSR analysis of seismic site effects and soil-structure resonance in Varaždin city (North Croatia). *Soil Dynamics and Earthquake Engineering*, 92, 666-677.

Tang, C., Zhu, J., Qi, X., & Ding, J. (2011). Landslides induced by the Wenchuan earthquake and the subsequent strong rainfall event: A case study in the Beichuan area of China. *Engineering Geology*, 122(1-2), 22-33.

Van Asch, T. W. J., & Malet, J. P. (2009). Flow-type failures in fine-grained soils: an important aspect in landslide hazard analysis. *Natural Hazards and Earth System Sciences,* 9(5), 1703-1711.

Vouillamoz, N., Rothmund, S., & Joswig, M. (2018). Characterizing the complexity of microseismic signals at slow-moving clay-rich debris slides: the Super-Sauze (southeastern France) and Pechgrabe (Upper Austria) case studies. *Earth Surface Dynamics*, 6(2).

Wibisana, A. (2013). *The myths of environmental compensation in Indonesia: lessons from the Sidoarjo mudflow.* In: Regulating Disasters, Climate Change and Environmental Harm. Edward Elgar Publishing.

Yunus, A. P., Fan, X., Tang, X., Jie, D., Xu, Q., & Huang, R. (2020). Decadal vegetation succession from MODIS reveals the spatio-temporal evolution of post-seismic landsliding after the 2008 Wenchuan earthquake. *Remote Sensing of Environment*, 236, 111476. https://doi.org/10.1016/j.rse.2019.111476

Zare, M. A., Haghshenas, E., & Jafari, M. K. (2017). Interpretation of dynamic response of a very complex landslide (Latian-Tehran) based on ambient noise investigation. *Soil Dynamics and Earthquake Engineering*, 100, 559-572.

Zhou, J. W., Cui, P., & Hao, M. H. (2016). Comprehensive analyses of the initiation and entrainment processes of the 2000 Yigong catastrophic landslide in Tibet, China. *Landslides,* 13, 39-54.

Zhou, J. W., Cui, P., Yang, X. G., Su, Z. M., Guo, X. J. (2013). Debris flows introduced in landslide deposits under rainfall conditions: The case of Wenjiagou gully. *Journal of Mountain Science,* 10, 249-260.